Journal of Biomechanics 88 (2019) 113–121

Contents lists available at ScienceDirect

Journal of Biomechanics

journal homepage: www.elsevier.com/locate/jbiomech
www.JBiomech.com

Layer-specific arterial micromechanics and microstructure: Influences of age, anatomical location, and processing technique

Michael Rafuse [a], Xin Xu [a], Kurt Stenmark [b], Corey P. Neu [a], Xiaobo Yin [a], Wei Tan [a,*]

[a] Department of Mechanical Engineering, University of Colorado Boulder, Boulder, CO 80309, USA
[b] Cardiovascular Pulmonary Research Laboratories, University of Colorado Anschutz Medical Campus, Aurora, CO 80045, USA

ARTICLE INFO

Article history:
Accepted 18 March 2019

Keywords:
Atomic force microscopy
Multiphoton microscopy
Collagen
Elastin
Glycosaminoglycans

ABSTRACT

The importance of matrix micromechanics is increasingly recognized in cardiovascular research due to the intimate role they play in local vascular cell physiology. However, variations in micromechanics among arterial layers (i.e. intima, media, adventitia), as well as dependency on local matrix composition and/or structure, anatomical location or developmental stage remain largely unknown. This study determined layer-specific stiffness in elastic arteries, including the main pulmonary artery, ascending aorta, and carotid artery using atomic force indentation. To compare stiffness with age and frozen processing techniques, neonatal and adult pulmonary arteries were tested, while fresh (vibratomed) and frozen (cryotomed) tissues were tested from the adult aorta. Results revealed that the mean compressive modulus varied among the intima, sub-luminal media, inner-middle media, and adventitia layers in the range of 1–10 kPa for adult arteries. Adult samples, when compared to neonatal pulmonary arteries, exhibited increased stiffness in all layers except adventitia. Compared to freshly isolated samples, frozen preparation yielded small stiffness increases in each layer to varied degrees, thus inaccurately representing physiological stiffness. To interpret micromechanics measurements, composition and structure analyses of structural matrix proteins were conducted with histology and multiphoton imaging modalities including second harmonic generation and two-photon fluorescence. Composition analysis of matrix protein area density demonstrated that decrease in the elastin-to-collagen and/or glycosaminoglycan-to-collagen ratios corresponded to stiffness increases in identical layers among different types of arteries. However, composition analysis was insufficient to interpret stiffness variations between layers which had dissimilar microstructure. Detailed microstructure analyses may contribute to more complete understanding of arterial micromechanics.

1. Introduction

Vascular tissue mechanics play a significant role in regulating vascular cell phenotypes and physiological activities (Mozos et al., 2017). For example, elastic artery stiffening is associated with increased risk of hypertension and stroke (Mitchell, 2014). While macroscopic analysis of arterial mechanics is well-developed now, there remains a limited understanding as to the contribution of cellular-scale mechanics to vascular health and disease (Arroyave et al., 2015; Kohn et al., 2015). Such understanding is vital as the artery wall consists of three distinct layers, the intima, media, and adventitia, each composed of a unique cell type and matrix microenvironment. Individual layers may thicken or stiffen independently with anatomical location, development, aging, or disease imposing varied influences on local cell activities. Therefore, layer-specific analysis at cellular length scales is important to understanding arterial mechanobiology, pathological remodeling, and tissue engineering (Cabrera-Fischer et al., 2013; Kohn et al., 2015; Stenmark et al., 2011; Townsley, 2012; Witter et al., 2017).

In the case of designing tissue-engineered constructs, the importance of matching micromechanical properties of supporting biomaterials with healthy arterial stiffness, in order to facilitate proper vascular cell function, is now being recognized (Ding et al., 2018). To this end, atomic force microscopy (AFM) indentation is used to measure artery mechanics (Grant and Twigg, 2013; Kohn et al., 2016; Liu et al., 2016; Peloquin et al., 2011). AFM enables mechanical analysis of hydrated biological tissues with high spatial resolution. There are wide variations, however, between the reported stiffness of different arterial layers. For example, reported AFM indentation measures of stiffness in the adventitial layer of porcine pulmonary arteries reveal a mean of 128.6 kPa, while stiffness measures in bovine carotid intima and

* Corresponding author at: 427 UCB, 1111 Engineering Dr. Boulder, CO 80309-0427, USA.
E-mail address: wtan@colorado.edu (W. Tan).

https://doi.org/10.1016/j.jbiomech.2019.03.026
0021-9290/

porcine carotid media layers had mean stiffness of 2.5 kPa and 5.7 kPa respectively (Engler et al., 2004; Grant and Twigg, 2013; Peloquin et al., 2011). However, function of vascular cells such as endothelial cells and smooth muscle cells, as well as vascular lineage differentiation from stem cells, are highly sensitive to small changes in extracellular matrix mechanics (Ding et al., 2018, 2017). Thus, to better understand arterial mechanobiology and inform arterial engineering, it is necessary to accurately quantify variations in layer-specific stiffness across the artery wall, as well as the influences of age, anatomical location, and processing prior to measurement of arterial tissue stiffness.

Herein, we measured the layer-specific, biomechanical properties of fresh pulmonary, aorta, and carotid arteries and investigated the relationship between layer-specific stiffness and structural matrix protein composition using AFM microindentation and multiphoton imaging techniques. Further, we examined the effects of tissue processing and age/development on the matrix micromechanics and microstructure.

2. Materials and methods

2.1. Tissue sample preparation

Adult bovine vessel segments from the main pulmonary artery, ascending aorta, and left common carotid artery were obtained immediately post mortem from Innovative Foods LLC (Evans, CO) where the age of slaughtered cattle was between 20 and 30 months (Fig. 1A). For neonatal samples, main pulmonary artery segments were harvested from three-week old calves (purchased from a local farm) and transported in PBS on ice. Standard veterinary care was used following institutional guidelines, and the procedure was approved by the Institutional Animal Care and Use Committee (University of Colorado Health Sciences Center, Denver, CO). Loose perivascular connective tissue from the outer adventitia was carefully removed and 4×6 mm artery wall sections were prepared for cross-sectioning. Throughout preparation, arteries were covered with chilled PBS.

To reveal individual arterial layers and measure their mechanical properties, a thin circumferential cross-section of the artery wall was used as described previously (Engler et al., 2004). For fresh (vibratomed) cross-sectioning, wall sections were embedded in 6% low gelling temperature agarose (Sigma A9045) at 35–40 °C (Fig. 1B). When solidified, the agarose with embedded tissue was bonded (Loctite SuperGlue) to a vibratome block and placed in the vibratome buffer tray filled with PBS and surrounded with ice. Sections (~200 μm) were cut with a vibratome (Leica VT1000S) at ~0.05 mm/s and 100 Hz. The thin cross-section was then removed from surrounding agarose and submerged in chilled PBS.

To identify possible effects of frozen preparation on matrix stiffness, wall sections from the aorta were also embedded in optimal

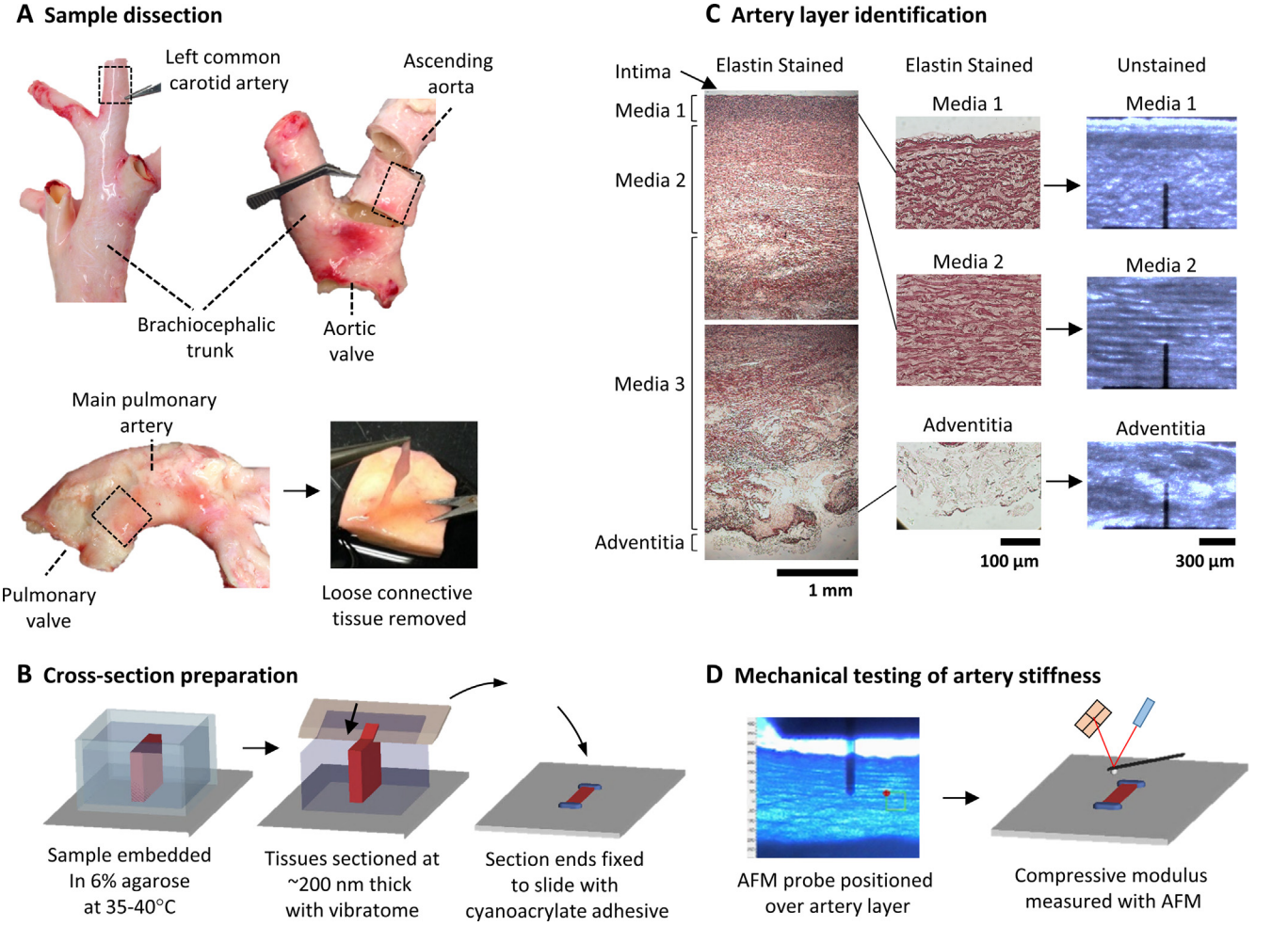

Fig. 1. Methods of preparing large elastic arteries for layer-specific stiffness measurement using atomic force microscopy. (A) Tissue samples taken from similar sites for each artery type – Left common carotid artery samples were collected ~1–3 cm after branching while aorta and pulmonary artery samples were collected from the lower curvature of the vessel. (B) Sample embedding, sectioning, and mounting. (C) Artery layers were visually identified to determine indentation test locations. Aorta samples shown. (D) The compressive modulus of each layer was measured 8 times at 3 locations to provide an estimate of layer-specific stiffness for each artery sample.

cutting temperature compound, placed on dry ice until frozen, and stored at −80 °C for up to 12 weeks. Samples were cryosectioned (~200 μm) using a cryotome, then immediately rinsed and submerged in chilled PBS to prevent drying.

For AFM indentation of medial and adventitial layers, a cross-section was mounted on a microscope slide by adding a small drop of SuperGlue adhesive to the ends of the sections, away from the testing regions. The sample was then rehydrated with PBS and rinsed. We compared the mechanical measures using adhesive mounting with those using clamps, showing no effect of adhesives on the results (Fig. S1). Samples with uneven surfaces were discarded. For intimal indentation, a section of the artery wall (~1 mm) was glued to the slide, with the intima facing up. Prior to indentation measures, cell viability tests using calcein-am and propidium iodide assays on representative samples revealed complete cell death throughout the artery wall.

2.2. AFM indentation measurements in multiple artery layers

Contact-mode microindentation was performed using a Keysight 5500 AFM System (Keysight Technologies Inc., Santa Rosa, CA, USA) coupled with a video microscope to visually identify individual arterial layers (Fig. 1C–D). Cantilever deflection sensitivity was first calibrated. Force-displacement measurements were taken at three different locations within each arterial layer. At each location, indentation measurements were taken in an array of 4 × 4 points within a 30 × 30 μm area using force-volume mode. Indentations were made into the tissue (typically 0.2–2.0 μm) using a 5 μm radius polystyrene bead attached to a rectangular cantilever probe (Novascan, Ames, IA, USA). The cantilever spring constant (k_c = 0.10 N/m) was calibrated by the manufacturer. The same probe was used for all AFM measures.

Tissues were indented at a rate of 3.89 μm/s until a trigger load signal of 3 V (~15 nN) was reached and the tip was withdrawn. All AFM measurements were obtained in PBS at room temperature within 10–15 h post-mortem. For cryosectioned samples, this includes the amount of time the sample was unfrozen. To estimate the compressive modulus, force-displacement approach curves (Fig. S2B) were fit to the Hertzian linear elastic contact model for a spherical indenter (Fig. S2A) (Fuhrmann et al., 2011; Johnson et al., 1971). PicoView 1.4 was used to estimate the compressive modulus assuming a Poisson's ratio of 0.5.

2.3. Analysis of structural proteins using histology and multiphoton imaging

For structural analysis, a 4 × 6 mm wall section was fixed in 10% formalin. Samples were dehydrated in graded ethanols, paraffin embedded, microtome sectioned at 5 μm, and mounted on glass slides. Slides were deparaffinized, hydrated with graded ethanols, and immersed in PBS. The slides were then covered with #1 coverslip, and imaged using a confocal laser scanning microscope system (Bio-Rad, Radiance 2000 MP) with a 40× magnification (N.A. = 1.30, oil). Multiphoton imaging modalities including second harmonic generation (SHG) and two-photon excitation fluorescence (TPEF) were used to quantify collagen and elastin respectively. The multiphoton imaging parameters are described in the Supplementary Materials section.

Traditional histological results were compared with multiphoton images. For elastin fibers, tissue sections were stained for 30 min with 1% (m/v) orcein dissolved in 45% acetic acid and then submerged in 70% ethanol alcohol for 30 min. Collagen content was visualized by staining sections with picrosirius red stain (0.1% m/v sirius red F3B in saturated aqueous picric acid) for one hour, and then rinsing in two changes of 0.5% acetic acid for two minutes each. Glycosaminoglycans were stained using 1% (m/v) alcian blue 8GX in 3% acetic acid and then rinsed in running water for two minutes. Stained samples were then dehydrated using graded ethanols and mounted on slides. Picrosirius red stain was imaged with cross-polarized light to illuminate the natural birefringence of collagen fibers. Brightfield microscopy was used to image the other stains. Images were captured from representative areas of each arterial layer using a 40× objective.

To quantify protein content of fibrillar collagen (SHG), elastin (TPEF), and glycosaminoglycans (alcian blue), a custom image analysis script was developed using the MATLAB image-processing toolbox. Protein content was calculated as the ratio of protein-positive pixels to total number of pixels for each image. The black and white conversion threshold was pre-determined for each protein type to best approximate protein-positive areas (Bauman et al., 2014; Koch et al., 2014). Care was taken to acquire images and quantify protein areas using similar conditions and parameters, as further described in the Supplementary Materials section.

2.4. Statistics

For AFM measurements, eight measures showing smooth and complete force-displacement curves were randomly selected from each 4 × 4 array. Statistical significance was determined using a mixed-effect model to account for repeated measurements from multiple locations measured in each arterial layer (Minitab 18.1 Software). Fixed effects included artery type and arterial layer, while random effects included individual animals and measurement locations within an arterial layer. Multiple comparisons were performed using the Bonferoni method. Statistical significance for protein density was determined using one-way ANOVA. Pairwise comparisons were performed using the Tukey method. Statistical significance was set at $p < 0.05$. Sample numbers are included in figure legends.

3. Results

3.1. Arterial tissue stiffness changes with the arterial layer, anatomical location, and age

Within the artery wall, matrix stiffness was determined on the intima surface, the sub-luminal media (media_1), the inner-middle media (media_2), and the adventitia. While the media layer of the ascending aorta and pulmonary arteries has a distinct "outer media" layer (media_3), comprising almost two-thirds of the total medial thickness, stiffness in this layer was not measured due to its highly irregular pattern of elastic fibers and large SMC clusters (Frid et al., 1994).

AFM indentation measures revealed that the compressive moduli of pulmonary artery, ascending aorta, and carotid artery were within a similar order of magnitude, with mean values ranging from 1.49 to 2.52 kPa, 1.47–2.52 kPa, and 1.32–8.30 kPa, respectively (Fig. 2). Though variation of the mean stiffness in each artery was small, distinct changes between arterial layers existed. Also, inter-layer stiffness variations across the artery wall (i.e. from intima to adventitia) followed unique patterns specific to the artery type. Inter-layer stiffness also varies among arteries of different generations, i.e. main pulmonary artery (1st generation), ascending aorta (1st generation), and carotid artery (3rd generation). With higher generation number, stiffness increases occurred in the media, rather than in the intima or adventitia. Additionally, inter-layer variations of matrix stiffness were smaller on first-generation arteries when compared to third-generation arteries.

AFM indentation in neonatal and adult main pulmonary artery revealed a significant increase in the intima (0.86–2.50 kPa),

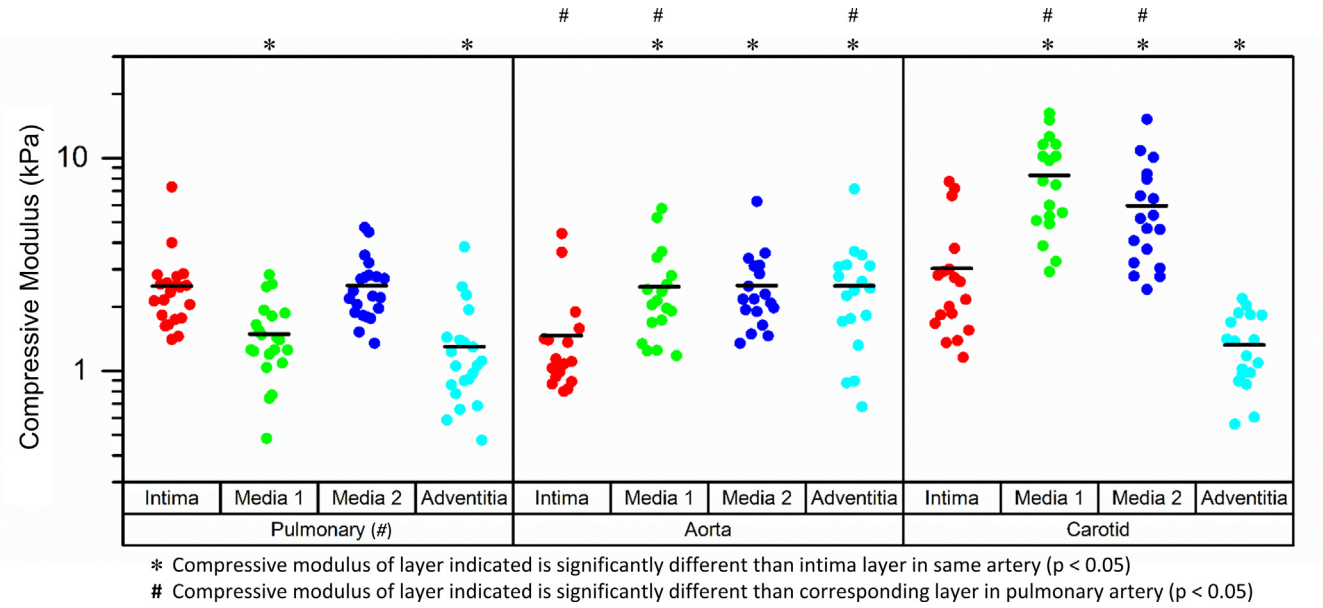

Fig. 2. Layer-specific stiffness measurements show distinct changes between individual layers of the main pulmonary artery, aorta, and carotid artery. Statistical significance was determined using a mixed effects model with multiple comparisons determined using the Bonferroni method. Arteries from six to seven animals were tested with three locations measured per layer and eight measurements at each location (30 × 30 μm). Each symbol represents the mean compressive modulus measured at one location.

media_1 (0.90–1.49 kPa) and media_2 (1.54–2.52 kPa) layers (Fig. 3). Interestingly, stiffness variations are not similar to adult tissue, suggesting that stiffening during juvenile development is primarily accompanied by arterial matrix remodeling in the intima and media layers.

3.2. Effects of storage or processing technique on layer-specific stiffness

Effects of frozen sample preparation on matrix stiffness were evaluated using cryosectioned tissues having similar thicknesses to vibratome-sectioned cross-sections. Results revealed frozen preparation caused statistically significant increases of mean stiffness values (Fig. 4) in the intima layer (Δ = 1.90 kPa) and media_2 layer (Δ = 3.01 kPa). This suggest that measures with frozen preparation, even with proper hydration before and after freezing, may not accurately represent the healthy physiological stiffness nor the variation in inter-layer stiffness.

3.3. Multiphoton and histological analysis of structural matrix proteins

Previous studies have shown that arterial matrix stiffness could be explained by an analysis of its passive structural components including fibrillar collagens (predominantly types I and III), elastin fibers, and glycoproteins (Robertson and Watton, 2013). These structural proteins also play diverse roles in pathological processes and disease-related changes in stiffness through their production, remodeling, and degradation (Mattson et al., 2017). Here we analyzed fibrillar collagens, elastin, and glycosaminoglycans. Multiphoton imaging modalities, SHG and TPEF, were used to simultaneously image unstained fibrillar collagen and elastin fibers respectively (Fig. 5A–C). Histological analysis for fibrillar collagen, elastin, and glycosaminoglycan content was performed and imaged using brightfield microscopy (Fig. 5D–F). Results from the histological imaging of fibrillar collagens and elastin were used to validate our multiphoton imaging results. Our initial multipho-

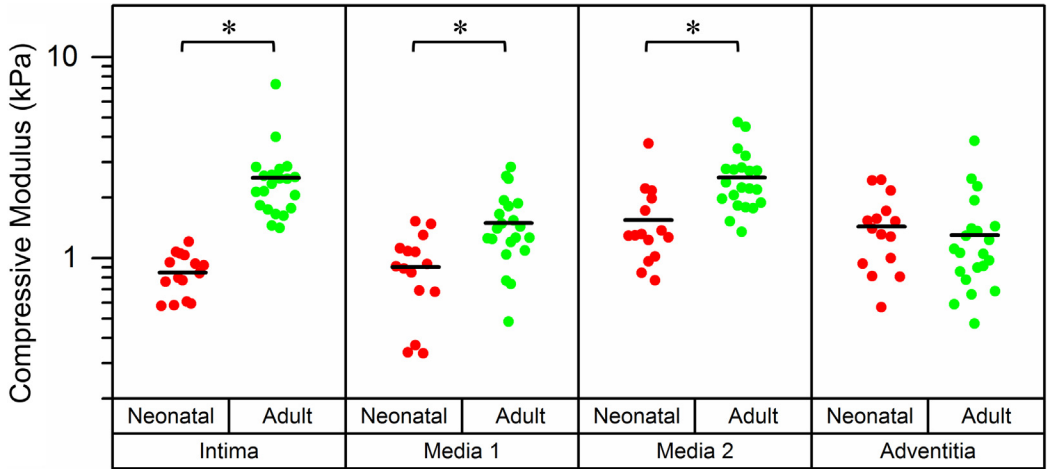

Fig. 3. Increased pulmonary artery stiffness from neonate to adult occurs in intima and media layers. Statistical significance was determined using a mixed effects model with multiple comparisons determined using the Bonferroni method. Arteries from two animals for neonatal, and seven animals for adult, were tested with three locations measured per layer and 8 measurements at each location (30 × 30 μm). Each symbol represents the mean compressive modulus measured at one location.

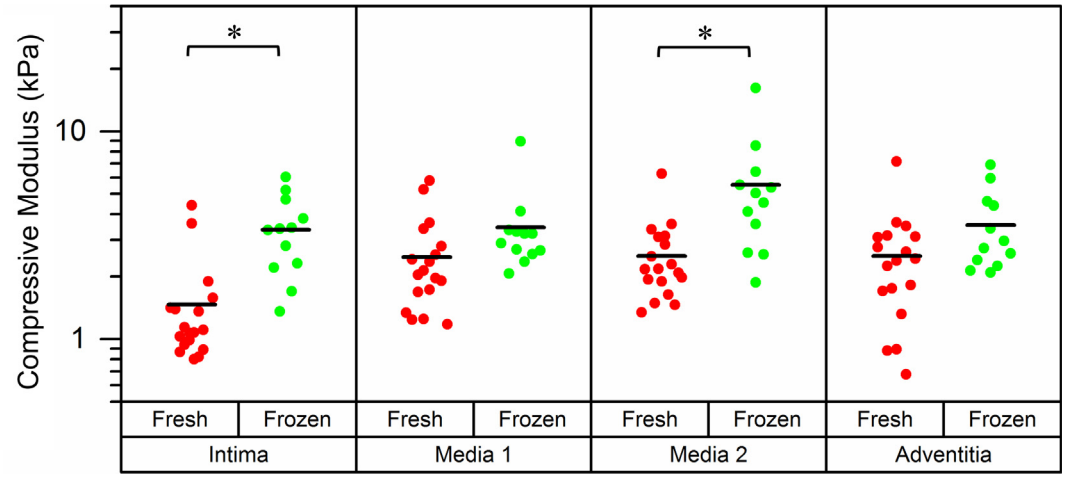

Fig. 4. Layer-specific stiffness measurements of fresh and frozen prepared tissue samples show non-uniform stiffening across layers of the aorta. Statistical significance was determined using a mixed effects model with multiple comparisons determined using the Bonferroni method. Samples from six unfrozen, and four frozen arteries were tested with three locations measured per layer and eight measurements per 30 × 30 μm location. Each symbol represents the mean compressive modulus at one location.

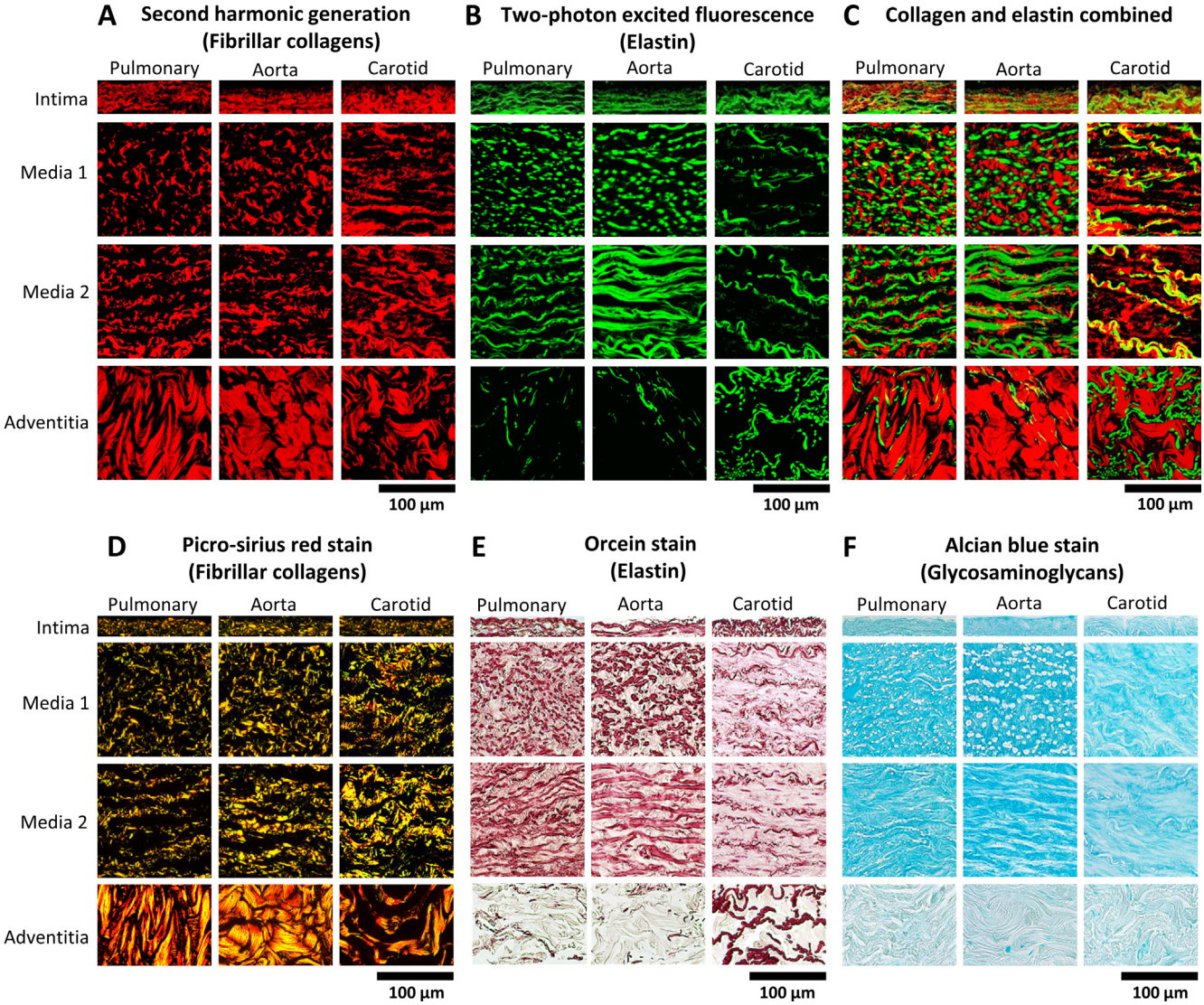

Fig. 5. Analysis of structural matrix protein content using SHG, TPEF, and histology. (A–C) Multiphoton images were used to analyze the protein area density for collagen (red) and elastin (green). (D–F) Histology images of collagen, elastin and glycosaminoglycans by staining samples with picrosirius red, orcein, and alcian blue stains, respectively. Scale bar for all images is 100 μm. (For interpretation of the references to colour in this figure legend, the reader is referred to the web version of this article.)

ton images, collected using conventional methods (Fig. S3), exhibited significantly less collagen and elastin than histological images. We discovered that the signal loss was primarily associated with mounting media (resin) and use of the internal (descanned) detectors. Improvements were thus made by using PBS hydrated artery cross-sections and direct detectors (non-descanned). Also, the laser power was increased to the highest possible level without damaging the tissue proteins (approximately 10% of nominal 1.40 W output power). Finally, since SHG signal from collagen III is much weaker than collagen I (Ranjit et al., 2015), our imaging optimization method became further necessary to accurately reveal the total fibrillar collagen content. Comparisons of stain-free multiphoton and histological stain imaging techniques demonstrated that multiphoton imaging with our system optimization yielded accurate information about fibrillar collagen and elastin content, with added benefits of higher resolution and specificity for quantification and microstructural analyses (Fig. S4).

To identify correlations between matrix composition and stiffness, quantification of protein-positive area was performed for collagen, elastin, and glycosaminoglycan areas (Fig. 6). Results showed an association between changes in matrix stiffness and protein composition. Specifically, increased stiffness in identical layers corresponded best to increased collagen-to-elastin ratio and/or decreased glycosaminoglycan-to-collagen ratio (Table 1). The same layer (e.g. media_1) in different artery types likely shares similar micro-structural organizations, for example, wavier, discontinuous fibrillar structures in media_1 compared to media_2.

Multiphoton (collagen and elastin) and histological (glycosaminoglycan) imaging of adult and neonatal pulmonary arteries was conducted to identify whether changes in protein content corresponded to increases in layer stiffness with age (Fig. 7). Interestingly, quantitative analysis of fibrillar collagen-to-elastin and glycosaminoglycan-to-collagen ratios did not correspond well to changes in layer stiffness. Rather, it was found that despite lower stiffness, neonatal tissues displayed significant increases in both collagen and elastin in the media layer and increased collagen content in the intima layer when compared to adult tissues (Table 2). Structural changes, however, were more evident. The lamellar structure in the media layer of adult tissues was better defined, with increased spacing for both elastin and fibrillar collagens. Furthermore, the orientation and fiber size of both elastin and collagen appear more homogeneous in adult pulmonary artery samples (Fig. 8).

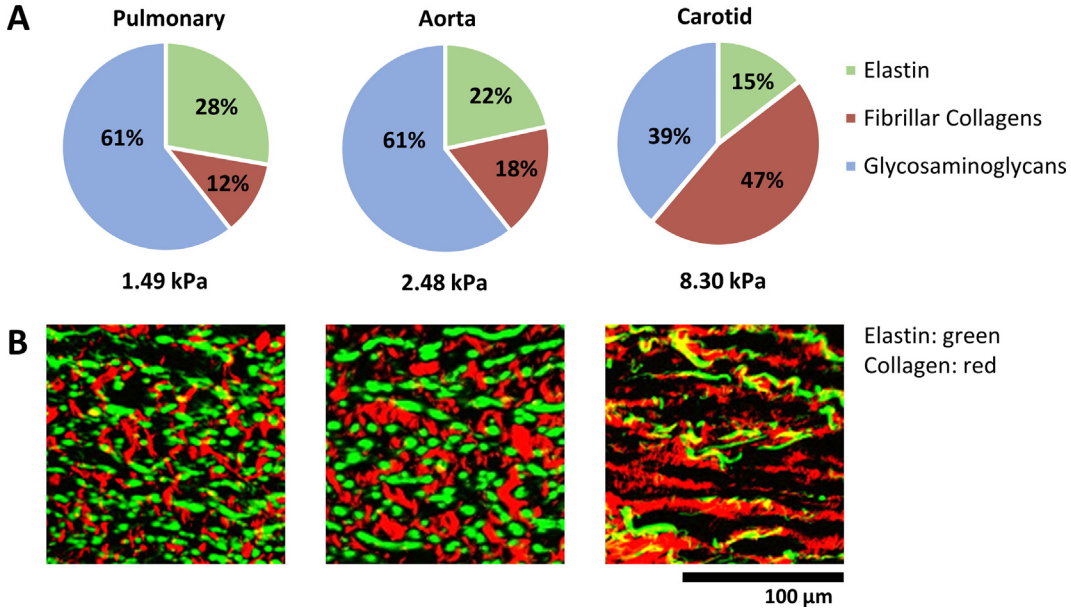

Fig. 6. (A) Normalized percent area of structural proteins in media_1 layer of pulmonary, aorta, and carotid arteries. Percentages represent area of elastin, fibrillar collagens, and glycosaminoglycan content when scaled to 100%. (B) Representative images of elastin (green) and collagen (red) in media_1 layer using multiphoton microscopy. (For interpretation of the references to colour in this figure legend, the reader is referred to the web version of this article.)

Table 1
Layer-specific ratios of fibrillar collagen-to-elastin and glycosaminoglycan-to-collagen proteins in pulmonary (P), aorta (A), and carotid (C) arteries.

	Fibrillar Collagen:Elastin				Glycosaminoglycan:Fibrillar Collagen			
Artery	Intima	Media 1	Media 2	Adventitia	Intima	Media 1	Media 2	Adventitia
Pulmonary	1.18 ± 0.18	0.43 ± 0.05	0.43 ± 0.07	6.97 ± 1.43	1.01 ± 0.29	5.24 ± 0.16	3.66 ± 0.86	0.13 ± 0.04
Aorta	1.04 ± 0.24	0.83 ± 0.08	0.34 ± 0.05	15.82 ± 2.79	1.44 ± 0.92	3.49 ± 0.28	2.66 ± 0.44	0.07 ± 0.01
Carotid	1.53 ± 0.23	3.64 ± 0.97	3.66 ± 0.67	1.66 ± 0.17	0.92 ± 0.19	0.82 ± 0.27	0.33 ± 0.18	0.17 ± 0.03
ANOVA	n.s.	p < 0.05	p < 0.05	p < 0.05	n.s.	p < 0.05	p < 0.05	n.s.
P-A	#	#		#*	#	#*		#
P-C		#*	#*			#*	# *	
A-C	#	#*	#*	#*	#	#*	#*	#

Note: Protein ratios are represented as mean ± SEM. Artery samples were imaged from 4 animals.
*Indicates protein ratios of the indicated artery pair are significantly different ($p < 0.05$). Statistical significance for each layer was first determined using a one-way ANOVA with pairwise comparisons performed using the Tukey method.
#Indicates layer stiffness is significantly different for the indicated artery pair ($p < 0.05$).

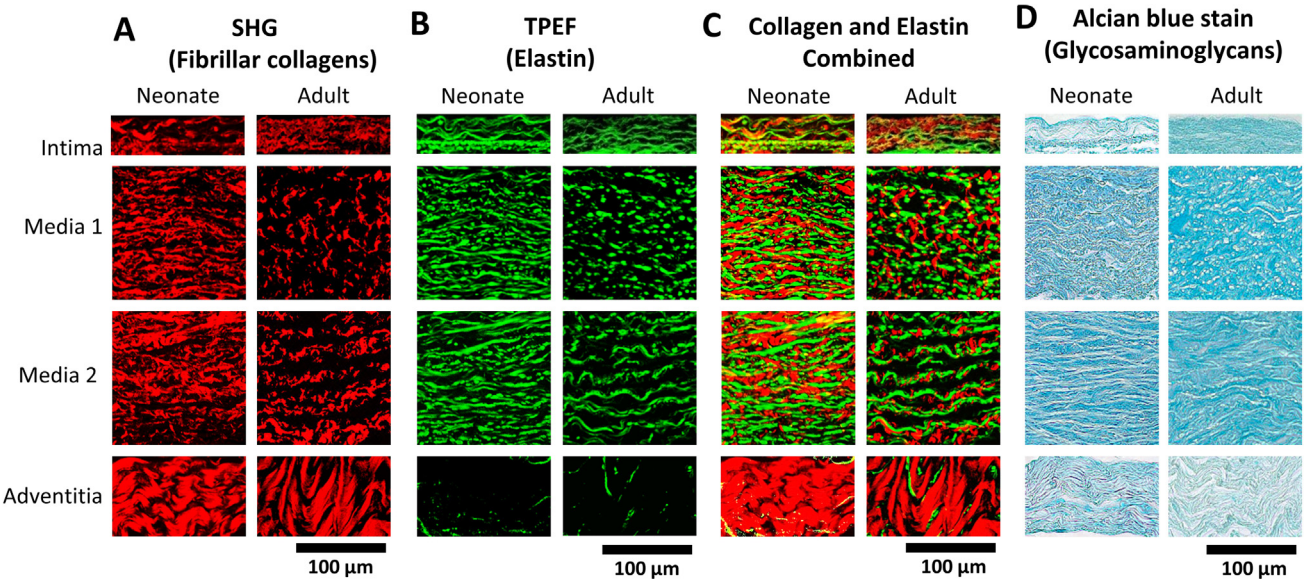

Fig. 7. Analysis of structural protein content using histology, SHG, and TPEF in neonatal and adult main pulmonary arteries. (A–C) Multiphoton images were used to calculate protein area density for collagen (red) and elastin (green). (D) Alcian blue staining was used to calculate glycosaminoglycan area density in each layer. Scale bar for all images above is 100 μm. (For interpretation of the references to colour in this figure legend, the reader is referred to the web version of this article.)

Table 2
Collagen, elastin, and glycosaminoglycan area ratios in neonatal and adult main pulmonary arteries.

	Fibrillar Collagen			
Age	Intima	Media 1	Media 2	Adventitia
Neonate	0.24 ± 0.02	0.41 ± 0.03	0.51 ± 0.04	0.82 ± 0.05
Adult	0.41 ± 0.04	0.11 ± 0.01	0.12 ± 0.02	0.42 ± 0.03
ANOVA	#*	#*	#*	*
	Elastin			
Age	Intima	Media 1	Media 2	Adventitia
Neonate	0.41 ± 0.03	0.48 ± 0.02	0.60 ± 0.03	0.03 ± 0.01
Adult	0.36 ± 0.04	0.26 ± 0.03	0.29 ± 0.01	0.07 ± 0.02
ANOVA	#	#*	#*	
	Glycosaminoglycan			
Age	Intima	Media 1	Media 2	Adventitia
Neonate	0.19 ± 0.01	0.25 ± 0.01	0.31 ± 0.01	0.16 ± 0.00
Adult	0.39 ± 0.07	0.58 ± 0.03	0.42 ± 0.04	0.05 ± 0.01
ANOVA	#	#*	#	*

Note: Protein area ratios are represented as mean ± SEM. Artery samples were tested from 4 locations per layer from 1 animal.
*Indicates protein area ratios of the indicated artery pair are significantly different ($p < 0.05$). Statistical significance for each layer was first determined using a one-way ANOVA with pairwise comparisons performed using the Tukey method.
#Indicates layer stiffness is significantly increased for the indicated artery pair ($p < 0.05$).

The non-uniform stiffening observed with frozen preparation and sectioning was not well explained by protein area density analysis. It is possible that temperature changes and the resulting water crystallization altered the micro/nano-structural organizations of matrix proteins, leading to inconsistent results.

4. Discussion

4.1. Micro-scale mechanics in elastic arteries

Using AFM microindentation, we were able to describe the variations in cellular-scale stiffness throughout the artery wall in elastic arteries. This demonstrated for the first time that while layer-specific stiffness in hydrated, unfrozen arterial tissue vary throughout the arterial wall, the expected variation is of a small order of magnitude, with inter-layer variations of mean compressive modulus not exceeding 7 kPa. This data suggests a range of physiological arterial stiffness on an order of magnitude around 1–10 kPa. Compared to recent measures using AFM microindentation, our measures of bovine carotid media (6.0–8.3 kPa) and intima (~3.8 kPa) resemble prior measures of porcine carotid media (~5–8 kPa) (Engler et al., 2004) and intima (2.5 ± 1.9 kPa) (Peloquin et al., 2011), respectively. Interestingly, prior measures of intima stiffness in mice using AFM microindentation showed greater stiffness at 25–30 kPa and 32 kPa (Huynh et al., 2011; Kohn et al., 2016). Our stiffness measures in bovine main pulmonary artery and aorta adventitia (1.36 kPa and 1.73 kPa respectively), however, were significantly lower than previous adventitial stiffness measures of similar tissues in porcine (129 kPa and 26 kPa respectively) (Grant and Twigg, 2013). Mechanical measurements of cryosectioned human and rat pulmonary arterioles by Liu

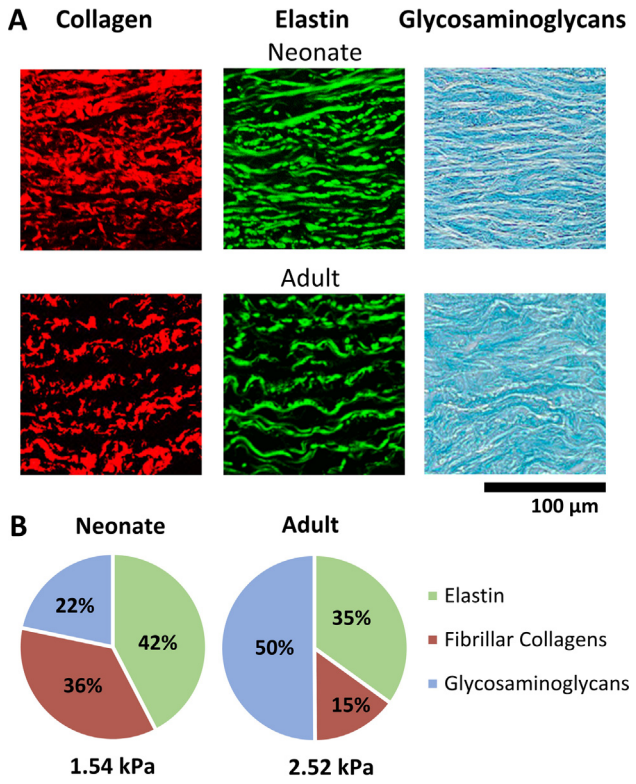

Fig. 8. Protein structure and composition analysis in media 2 layer of neonatal and adult main pulmonary artery. (A) Protein content and structure is visualized using multiphoton and brightfield microscopy. (B) Normalized percent area of structural proteins. Scale bar for all images above is 100 μm.

et al. (2016) suggest that use of cryosectioning with prompt rehydration may help maintain mechanical properties within physiological orders of magnitude. It is possible that discrepancies with previous studies arise from the use of frozen preparation with delayed rehydration after cryosectioning or differences in measurement parameters. The stiffness changes between arteries of different generations might be due to (a) the different matrix production by the cells in response to varied flow pulsations, and (b) the different physiological roles that they serve in the arterial tree.

4.2. Correlation between matrix micromechanics and protein composition

To identify possible relations between protein composition and matrix stiffness, we quantified the area density of primary structural matrix components, which are known to contribute to matrix permeability, hydration and mechanics (Beenakker et al., 2012). Our results revealed that decreased elastin-to-collagen and/or glycosaminoglycan-to-collagen ratios corresponded well to the increased stiffness in the identical arterial layers among different artery types (e.g. media_1 in pulmonary and carotid arteries), as illustrated in Fig. S5 and Table S1. Interestingly, no such matrix stiffness-composition correlation was found in the inter-layer stiffness variations (e.g. between media_2 and adventitia in the same artery) or in the comparison of layer-specific stiffness between neonatal and adult pulmonary arteries. The results imply that the arterial matrix stiffness-composition correlation only applies to arterial tissue composites with similar micro/nano-structures such as fibrillar alignment and crosslinking structures. When the matrix structures differ with arterial layer or age, more comprehensive analyses over the matrix structures must be considered. The significant structural variations in matrix proteins, such as fiber size and orientation, are evident between different layers (Chow et al., 2014; Robertson and Watton, 2013). Similarly, our study also suggests that small but statistically significant increases (i.e. 1–2 kPa) in the intima and media stiffness during juvenile development (e.g. neonatal vs adult pulmonary arteries) is likely due to significant changes in matrix structure during neonate to adult development. Therefore, while our results are in agreement with previous studies suggesting increased collagen-to-elastin ratios correspond to increased matrix stiffness (or decreased vessel compliance) in elastic arteries (Bender et al., 2015; Dodson et al., 2013; Xu et al., 2010), we also showed (a) glycosaminoglycan-to-collagen ratio as an additional factor describing the contribution of the matrix protein content, and (b) matrix microstructure as the major contributor to arterial matrix micromechanics for structurally-distinct arterial tissues.

4.3. Stiffening effects of frozen storage and preparation

Since discrepancies between our stiffness measures and prior studies could derive from different tissue processing techniques, we prepared fresh and frozen samples from each aorta to examine changes due to frozen storage and cryosectioning. While our measures revealed non-uniform increases in matrix stiffness, with significant changes occurring in the intima (+2 kPa) and media_2 (+3 kPa), they did not explain the significantly higher measures, found with other frozen preparation protocols (Akhtar et al., 2009; Beenakker et al., 2012; Grant and Twigg, 2013). These significant discrepancies could result from differences in measurement parameters such as probe size and shape. Sample dehydration or matrix-water interactions during the tissue freezing-thawing process might further contribute to variations in measurement results. While our results indicate that frozen preparation can increase matrix stiffness even with immediate rehydration, the increase is small enough that all layers remain at a similar order of magnitude. These results indicate that proper storage, sectioning, and hydration conditions can minimize changes from freezing and allow for comparison analysis of samples while expecting small increases from physiological levels. The effect of the freeze-thaw cycle on micromechanics may be further influenced by the freezing temperature, likely due to the structural changes that can occur at lower temperatures or with wrinkling in cryosectioning (Xu et al., 2016). While freezing and storing arterial tissues up to 3 weeks at −20 °C has been shown to cause increases of ~20% in Young's modulus, Hemmesizadeh et al. found that storing artery tissues at −80 °C for up to 3 weeks caused an insignificant increase (~10%) in mean artery stiffness (Hemmasizadeh et al., 2012). Because vascular cells sense and differentiate subtle changes in matrix micromechanics, the accurate stiffness value of individual arterial layers may be crucial for arterial cell function or tissue regeneration.

4.4. Limitations

The Hertz model approximates an indented sample as a linear elastic, isotropic, and homogeneous solid described as an infinite half-plane. While soft tissue stiffness is commonly estimated using the Hertz model, the artery matrix is a heterogeneous composite, with non-isotropic and viscoelastic behavior (Chen and Kassab, 2016; Grant and Twigg, 2013). We attempted to decrease error by using the same indentation rate for all measures, testing with the probe fully submerged, and indenting each sample at multiple locations in each layer, with maximum indentation 1–2% of sample thickness. This study did not consider the contributions from physiologic blood pressure, active cell strains, or cell-matrix adhesions. Since these forces pre-load matrix proteins, our measures may not reflect physiologic matrix stiffness. Future work would benefit

from improved analysis to include these active contributions. Finally, this study only examines the microstructures of major matrix proteins, neglecting significant contributions of other molecular structures such as collagen cross-linking, which also have significant impact on matrix mechanics (Dodson et al., 2013; Kohn et al., 2016; Robertson and Watton, 2013).

Acknowledgements

This research was funded by NIH (NHLBI R01HL119371 to W. Tan). We would also like to thank PhD student Sabrina David (Materials Science and Engineering Laboratory of the Department of Mechanical Engineering at University of Colorado, Boulder) for training and assistance with use of the multiphoton imaging system, Dr. Maria Frid (Cardiovascular Pulmonary Research Laboratory at University of Colorado, Denver) for her instruction in identification of artery layers and dissection of artery samples, Dr. Brian Aguado and Prof. Kristi Anseth (Department of Chemical and Biological Engineering and the BioFrontiers Institute) for their training and assistance with their cryomicrotome system at the University of Colorado – Boulder.

Conflict of interest statement

The authors have no conflicts of interest to report.

Appendix A. Supplementary material

Supplementary data to this article can be found online at https://doi.org/10.1016/j.jbiomech.2019.03.026.

References

Akhtar, R., Schwarzer, N., Sherratt, M.J., Watson, R.E.B., Graham, H.K., Trafford, A.W., Mummery, P.M., Derby, B., 2009. Nanoindentation of histological specimens. J. Mater. Res. 24, 638–646. https://doi.org/10.1557/JMR.2009.0130.

Arroyave, G.A.I., Lima, R.G., Martins, P.A.L.S., Ramião, N., Jorge, R.M.N., 2015. Methodology for mechanical characterization of soft biological tissues: arteries. Procedia Eng. 110, 74–81. https://www.sciencedirect.com/science/article/pii/S1877705815012539.

Bauman, T.M., Nicholson, T.M., Abler, L.L., Eliceiri, K.W., Huang, W., Vezina, C.M., Ricke, W.A., 2014. Characterization of fibrillar collagens and extracellular matrix of glandular benign prostatic hyperplasia nodules. PLoS One, 9, p. e109102. https://doi.org/10.1371/journal.pone.0109102.

Beenakker, J.-W.M., Ashcroft, B.A., Lindeman, J.H.N., Oosterkamp, T.H., 2012. Mechanical properties of the extracellular matrix of the aorta studied by enzymatic treatments. Biophys. J . 102, 1731–1737. https://doi.org/10.1016/j.bpj.2012.03.041.

Bender, S.B., Castorena-Gonzalez, J.A., Garro, M., Reyes-Aldasoro, C.C., Sowers, J.R., DeMarco, V.G., Martinez-Lemus, L.A., 2015. Regional variation in arterial stiffening and dysfunction in Western diet-induced obesity. Am. J. Physiol. Heart Circ. Physiol. 309, H574–H582.

Cabrera-Fischer, E.I., Bia, D., Zócalo, Y., Wray, S., Armentano, R., 2013. The adventitia layer modulates the arterial wall elastic response to intra-aortic counterpulsation: in vivo studies. Artif. Organs 37, 1041–1048. https://doi.org/10.1111/aor.12111.

Chen, H., Kassab, G.S., 2016. Microstructure-based biomechanics of coronary arteries in health and disease. J. Biomech. 49, 2548–2559. https://doi.org/10.1016/j.jbiomech.2016.03.023.

Chow, M.-J., Turcotte, R., Lin, C.P., Zhang, Y., 2014. Arterial Extracellular matrix: a mechanobiological study of the contributions and interactions of elastin and collagen. Biophys. J. 106, 2684–2692. https://doi.org/10.1016/j.bpj.2014.05.014.

Ding, Y., Floren, M., Tan, W., 2017. High-throughput screening of vascular endothelium-destructive or protective microenvironments: cooperative actions of extracellular matrix composition, stiffness, and structure. Adv. Healthcare Mater. 6, 1601426. https://doi.org/10.1002/adhm.201601426.

Ding, Y., Xu, X., Sharma, S., Floren, M., Stenmark, K., Bryant, S.J., Neu, C.P., Tan, W., 2018. Biomimetic soft fibrous hydrogels for contractile and pharmacologically responsive smooth muscle. Acta Biomaterialia. https://doi.org/10.1016/j.actbio.2018.05.015.

Dodson, R.B., Rozance, P.J., Fleenor, B.S., Petrash, C.C., Shoemaker, L.G., Hunter, K.S., Ferguson, V.L., 2013. Increased arterial stiffness and extracellular matrix reorganization in intrauterine growth–restricted fetal sheep. Pediatr. Res. 73, 147–154. https://doi.org/10.1038/pr.2012.156.

Engler, A.J., Richert, L., Wong, J.Y., Picart, C., Discher, D.E., 2004. Surface probe measurements of the elasticity of sectioned tissue, thin gels and polyelectrolyte multilayer films: correlations between substrate stiffness and cell adhesion. Surf. Sci. 570, 142–154. https://doi.org/10.1016/j.susc.2004.06.179.

Frid, M.G., Moiseeva, E.P., Stenmark, K.R., 1994. Multiple phenotypically distinct smooth muscle cell populations exist in the adult and developing bovine pulmonary arterial media in vivo. Circ. Res. 75, 669–681. https://doi.org/10.1161/01.RES.75.4.669.

Fuhrmann, A., Staunton, J.R., Nandakumar, V., Banyai, N., Davies, P.C.W., Ros, R., 2011. AFM stiffness nanotomography of normal, metaplastic and dysplastic human esophageal cells. Phys. Biol. 8, 015007. https://doi.org/10.1088/1478-3975/8/1/015007.

Grant, C.A., Twigg, P.C., 2013. Pseudostatic and dynamic nanomechanics of the tunica adventitia in elastic arteries using atomic force microscopy. ACS Nano 7, 456–464. https://doi.org/10.1021/nn304508x.

Hemmasizadeh, A., Darvish, K., Autieri, M., 2012. Characterization of changes to the mechanical properties of arteries due to cold storage using nanoindentation tests. Ann. Biomed. Eng. 40, 1434–1442. https://doi.org/10.1007/s10439-011-0506-z.

Huynh, J., Nishimura, N., Rana, K., Peloquin, J.M., Califano, J.P., Montague, C.R., King, M.R., Schaffer, C.B., Reinhart-King, C.A., 2011. Age-related intimal stiffening enhances endothelial permeability and leukocyte transmigration. Sci. Transl. Med. 3, 112ra122. https://doi.org/10.1126/scitranslmed.3002761.

Johnson, K.L., Kendall, K., Roberts, A.D., 1971. Surface energy and the contact of elastic solids. The Royal Society, 301–313.

Koch, R.G., Tsamis, A., D'Amore, A., Wagner, W.R., Watkins, S.C., Gleason, T.G., Vorp, D.A., 2014. A custom image-based analysis tool for quantifying elastin and collagen micro-architecture in the wall of the human aorta from multi-photon microscopy. J. Biomech. 47, 935–943. https://doi.org/10.1016/j.jbiomech.2014.01.027.

Kohn, J.C., Chen, A., Cheng, S., Kowal, D.R., King, M.R., Reinhart-King, C.A., 2016. Mechanical heterogeneities in the subendothelial matrix develop with age and decrease with exercise. J. Biomech. 49, 1447–1453. https://doi.org/10.1016/j.jbiomech.2016.03.016.

Kohn, J.C., Lampi, M.C., Reinhart-King, C.A., 2015. Age-related vascular stiffening: causes and consequences. Front. Genet. 6. https://doi.org/10.3389/fgene.2015.00112.

Liu, F., Haeger, C.M., Dieffenbach, P.B., Sicard, D., Chrobak, I., Coronata, A.M.F., Suárez Velandia, M.M., Vitali, S., Colas, R.A., Norris, P.C., Marinković, A., Liu, X., Ma, J., Rose, C.D., Lee, S.-J., Comhair, S.A.A., Erzurum, S.C., McDonald, J.D., Serhan, C.N., Walsh, S.R., Tschumperlin, D.J., Fredenburgh, L.E., 2016. Distal vessel stiffening is an early and pivotal mechanobiological regulator of vascular remodeling and pulmonary hypertension. JCI Insight 1. https://doi.org/10.1172/jci.insight.86987.

Mattson, J.M., Turcotte, R., Zhang, Y., 2017. Glycosaminoglycans contribute to extracellular matrix fiber recruitment and arterial wall mechanics. Biomech. Model. Mechanobiol. 16, 213–225. https://doi.org/10.1007/s10237-016-0811-4.

Mitchell, G.F., 2014. Arterial stiffness and hypertension: chicken or egg? Hypertension 64, 210–214. https://doi.org/10.1161/HYPERTENSIONAHA.114.03449.

Mozos, I., Malainer, C., Horbańczuk, J., Gug, C., Stoian, D., Luca, C.T., Atanasov, A.G., 2017. Inflammatory markers for arterial stiffness in cardiovascular diseases. Front Immunol. 8. https://doi.org/10.3389/fimmu.2017.01058.

Peloquin, J., Huynh, J., Williams, R.M., Reinhart-King, C.A., 2011. Indentation measurements of the subendothelial matrix in bovine carotid arteries. J. Biomech. 44, 815–821. https://doi.org/10.1016/j.jbiomech.2010.12.018.

Ranjit, S., Dvornikov, A., Stakic, M., Hong, S.-H., Levi, M., Evans, R.M., Gratton, E., 2015. Imaging fibrosis and separating collagens using second harmonic generation and phasor approach to fluorescence lifetime imaging. Sci. Rep. 5. https://doi.org/10.1038/srep13378.

Robertson, A.M., Watton, P.N., 2013. Mechanobiology of the arterial wall. Modeling of transport in biological media. Elsevier, New York, pp. 275–347.

Stenmark, K.R., Nozik-Grayck, E., Gerasimovskaya, E., Anwar, A., Li, M., Riddle, S., Frid, M., 2011. The adventitia: essential role in pulmonary vascular remodeling. Compr. Physiol. 1, 141–161. https://doi.org/10.1002/cphy.c090017.

Townsley, M.I., 2012. Structure and composition of pulmonary arteries, capillaries and veins. Compr. Physiol. 2, 675–709. https://doi.org/10.1002/cphy.c100081.

Witter, K., Tonar, Z., Schöpper, H., 2017. How many layers has the adventitia? Structure of the arterial tunica externa revisited. Anat. Histol. Embryol. 46, 110–120. https://doi.org/10.1111/ahe.12239.

Xu, Q., Chakravorty, A., Bathgate, R.A.D., Dart, A.M., Du, X.J., 2010. Relaxin therapy reverses large artery remodeling and improves arterial compliance in senescent spontaneously hypertensive rats. Hypertension 55, 1260–1266. https://doi.org/10.1161/HYPERTENSIONAHA.109.149369.

Xu, X., Li, Z., Cai, L., Calve, S., Neu, C.P., 2016. Mapping the nonreciprocal micromechanics of individual cells and the surrounding matrix within living tissues. Sci. Rep. 6, 24272. https://doi.org/10.1038/srep24272.